Spread and Recoiling of Liquid Droplets Impacting Solid Surfaces

Xuan Gao and Ri Li
Dept. of Mechanical Engineering, School of Engineering, University of British Columbia, Kelowna, BC V1V 1V7, Canada

DOI 10.1002/aic.14440
Published online March 18, 2014 in Wiley Online Library (wileyonlinelibrary.com)

The impact of water droplets on solid surfaces is studied experimentally and theoretically. Theoretical equations based on energy conservation are developed. In our theoretical study, the droplet is modeled as a ring-like shape, which matches the dynamic shape of droplets observed from our experimental tests. In the analysis of energy conservation, the nonuniform distribution of pressure inside the deformed droplet is taken into account by introducing a flow potential energy term in the theoretical equations. To derive viscous dissipation for recoiling, a viscous layer coefficient is introduced. Its values for the tests using smooth surfaces are found to be within a small range. Both theoretical predictions and experimental data show significant influence of surface wettability on maximum spread and recoiling process. With the increase of advancing contact angle, surface energy shows a decreasing trend, whereas flow potential energy shows an increasing trend and becomes significant for hydrophobic surfaces. © 2014 American Institute of Chemical Engineers *AIChE J*, 60: 2683–2691, 2014

Keywords: droplet impact, spread diameter, recoiling, surface wettability, analytical model

Introduction

Controlled deposition of droplets is essential to many emerging applications such as ink-jet printing, microfabrication, rapid prototyping, and electronic packaging. The development of these technologies relies on good understanding of droplet dynamics during impact. In recent decades, study of droplet impact on solid surfaces has drawn much attention. The process of a liquid drop impacting a smooth, dry, and solid surface was divided by Rioboo et al.[1] into five successive phases: kinematic, spreading, relaxation, wetting, and equilibrium. Most research work has been focused on spreading and relaxation.

In the spreading phase, contact line expands radially until reaching a maximum spread diameter, which is determined by droplet initial diameter, impact velocity, surface tension, viscosity, and wettability of the solid surface.[2] The maximum spread diameter is of critical importance in spreading phase, which has been widely investigated by many researchers[2–8] using experimental and theoretical methods. Clanet et al.[3] found that the maximal spread on a superhydrophobic surface was significantly dependent on the viscosity of liquid droplets. The maximum spread of an impacting droplet in the capillary regime was found to scale with the Weber number, *We*, while the maximum spread in viscous regime could be plotted as a function of the Reynolds number, *Re*. Transition to the viscous regime was found when the impact number $P = We/Re^{4/5} > \sim 1$. van Dam and Clerc[4] found significant difference of maximum spread between substrates with small and large contact angles, which indicates the influence of surface wettability in the later stage of impact. Park et al.[5] further demonstrated the effects of surface tension, kinetic energy, and viscous dissipation on the impact process. These effects should be considered in practical applications and generally organized into the Reynolds and Weber numbers.

Some analytical models[6–10] were proposed to predict impaction process, in particular for maximum spread. Most models are based on the energy conservation of the droplet. Since Engel[6] developed the first correlation equation, efforts have been made to improve the accuracy of theoretical prediction. Chandra and Avedisian[7] developed an empirical correlation of viscous dissipation, which includes estimated spreading time, simplified dissipation function, and estimated volume of viscous dissipation. Improved predictive equations for viscous dissipation was presented by Mao et al.[8] The model after improvement could provide more accurate prediction of maximum spread for most cases except for low Reynolds and Weber numbers. It was demonstrated that the theoretical model based on assuming the droplet shape as a cylindrical disk at the maximum extension does not fit with experiments well in some cases. Other models developed by Park et al.[5] and Li et al.[2] show improvement for low Reynolds and Weber numbers. The droplet shape used in the two studies is a spherical cap instead of a cylindrical disk.

After spreading to a maximum extent, the contact line recedes, and even rebound can commonly appear in superhydrophobic surfaces if the initial kinetic energy is large enough. Most researchers focused on the impact process from the initial stage to the maximum spread, leading to incomplete understanding of the dynamics of the recoiling

Correspondence concerning this article should be addressed to R. Li at sunny.li@ubc.ca.

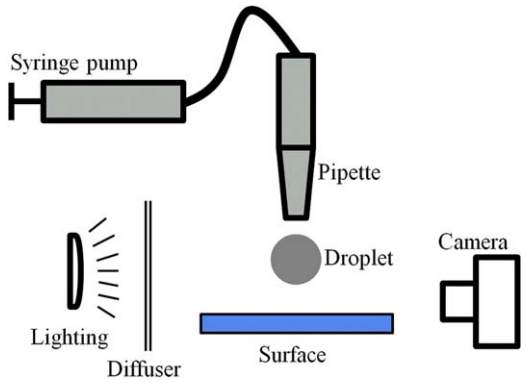

Figure 1. Schematic of experimental setup.

[Color figure can be viewed in the online issue, which is available at wileyonlinelibrary.com.]

process. Some studies[9–13] involved oscillatory motions of droplets after impacting solid surfaces. Pasandideh-Fard et al.[9] used a numerical solution of the Navier–Stokes equation with a modified SOLA-VOF (Solution Algorithm-Volume of Fluid) method to model the droplet impact. The droplet spread diameter during the recoiling process was overpredicted. Based on the approach proposed by Kendall and Rohsenow[10] and Bechtel et al.,[11] Kim and Chun[12] developed approximate theoretical models by using the variational principle. The results showed that the recoiling behavior of the droplets is determined by Weber number, Ohnesorge number, and equilibrium contact angle. Two geometric shapes were considered. The cylinder model was found to be suitable for droplet impact with small values of Ohnesorge number, whereas the truncated-sphere model agrees with experiments fairly well for high values of Ohnesorge number. Recently, Roisman et al.[13] introduced a strictly theoretical model to predict the evolution of spread diameter by analyzing the motion of a rim appearing at the edge of the liquid film. It was found that although no empirical parameter was used, the model could be in good agreement with the experimental data for $Re \gg We \gg 1$.

Although a number of studies involved spread and recoiling of liquid droplets on solid surfaces, studies based on actual dynamic shapes are limited. In our theoretical study, the droplet is modeled as a ring-like shape, which has a central thin film surrounded by semicircular rim. The assumed shape matches the dynamic shape of droplets observed from our experimental tests. The analytical model derived from energy conservation predicts maximum spread and recoiling processes of liquid droplets impacting solid surfaces, which is compared with the experimental results of different impacting conditions. In the analysis of energy conservation, the nonuniform distribution of pressure inside the deformed droplet is taken into account by introducing a flow potential energy term in the theoretical equations. To derive viscous dissipation for recoiling, a viscous layer coefficient is introduced. By fitting with experimental data, its value is found to vary in a small range for smooth surfaces. To understand surface effect, two types of reversible energy at the maximum spread, namely excessive surface energy and flow potential energy, are evaluated for droplets with varied impact conditions.

Experimental Methodology and Observation

Figure 1 shows experimental setup schematically. Small water droplets were generated from glass pipettes connected to a micropump. A slight pressure supplied by the pump was applied to the syringe and the plunger advanced very slowly to form a droplet at the tip of the pipette, which finally detached from the pipette under its own weight. Droplet size was changed by using different pipettes, and droplets with the diameters of 2 and 3.84 mm were tested. Droplet diameter was measured from the droplet images before impact. The height of the pipettes above the test surfaces was adjusted to change impact velocities. Three impact velocities were tested, 1.6, 2, and 2.2 m/s. They were calculated from droplet displacement and time interval between consecutive frames of high-speed video before impacting the solid surface.

Smooth aluminum surfaces with average roughness less than 0.1 μm were coated with varied selfassembled monolayers (SAM) to achieve varied hydrophilic and hydrophobic surfaces.[14] A superhydrophobic surface was also made by laser milling microtexture on the surface (10 μm square posts with spacing and depth being 10 μm) and coated with hydrophobic SAM. Advancing and receding contact angles were measured using the sessile drop method, which ranged from 10° to 155°.

As shown in Figure 1, a lamp served as an illumination source, and a diffuser was positioned in front of the lamp to produce uniform lighting. A high-speed camera (Phantom Miro M310, Vision Research) was used to record the spread and recoiling of droplets on surfaces. In the tests, the recording speed of the camera was usually set to be 2000 frames per second with shutter speed up to 1 μs.

Typical observation of water droplet impact in this work can be described based on Figure 2, which shows a droplet with 3.84 mm in diameter and velocity of 1.6 m/s impacting a surface with advancing and receding contact angles being 120° and 100° at room temperature. At the early stage of impact, the droplet deforms and spreads radially, and the center height decreases. More fluid is moving toward the

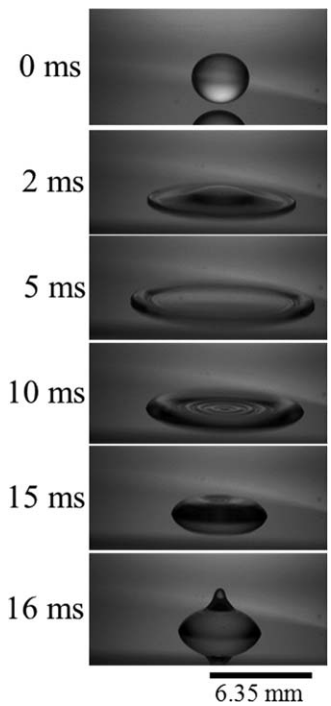

Figure 2. Impact of droplet ($U = 1.6$ m/s; $D = 3.84$ mm) on a smooth surface ($\theta_a = 120°$; $\theta_r = 100°$).

edge and the central part flattens. The spreading is driven by the rapid pressure increase at the point of impact after the droplet reaches the solid surface.[15] The impact velocity decreases rapidly from initial velocity to zero in a crashing time, and the typical deceleration during the drop impact is commonly two orders of magnitude higher than gravity.[3] It is apparent that the radial displacement of contact line from 0 to 2 ms is greater than that from 2 to 5 ms. The initial velocity of liquid spreading on the surface is usually greater than the initial impact velocity. Horizontally, the spreading velocity of contact line initially increases with increasing spread diameter up to a maximum level and then decreases. The decrease in velocity is caused both by surface tension and viscosity until reaching the maximum extent. Eventually, the advance of contact line stops, and the droplet becomes a ring-like shape, which has most fluid in its cylindrical edge and a thin film within the ring. The contact angle at this moment is equal to the measured advancing contact angle. This is called maximum spread. In Figure 2, the droplet spreads at the maximum extent at 5 ms. At maximum spread, the fluid is not at rest, because internal fluid motion still exists inside as revealed by Clanet et al.[3]

It is noted that recoiling does not start immediately after the spread process is complete. As shown in Figure 2, after reaching the maximum spread, local contact angle decreases toward receding contact angle. Once receding contact angle is reached, contact line starts moving inward. The ring-like shape remains, but the rim becomes thicker, and the film becomes smaller. Once the central film disappears, radially flowing-inward fluid impinges at the center, causing upward flow. After 16 ms, the droplet continues to develop to a liquid column. In the theoretical model, Fukai et al.[16] found that the surface energy accumulated during spreading has significant effects on upward bulk motion and subsequent oscillation. Droplets were observed to rebound easily on very hydrophobic surfaces.[17]

Theoretical Analysis

For the theoretical study of droplet impact, the assumption of droplet shape is of critical importance for the accuracy of theoretical prediction. Previous models usually used two kinds of droplet shapes: a cylindrical disk and a spherical cap. The cylindrical disk assumption is preferable due to its simplicity. Based on this geometric shape, the prediction of maximum spread was in good agreement with experiments for high Reynolds and Weber numbers, which was validated by Mao et al.[8] and Fukai et al.[18] However, for droplet impact with low velocities and high contact angles, the assumption of cylindrical disk leads to overprediction of maximum spread. It was shown that assuming a spherical cap provides improved prediction of maximum spread for low impact velocities.[5] For recoiling process, the cylinder model is good for droplets with small Ohnesorge numbers, whereas the sphere model is good for large Ohnesorge numbers.[12] Therefore, these two assumptions of droplet shape definitely have their limitation for predicting spread and recoiling processes.

In this work, we consider the actual shape that was observed from the experiments, which greatly differs from the previous models. The present model is schematically depicted in Figure 3. The droplet maintains a ring-like shape both at maximum spread (see 5 ms in Figure 2) and during the subsequent recoiling. The ring-like shape can be further

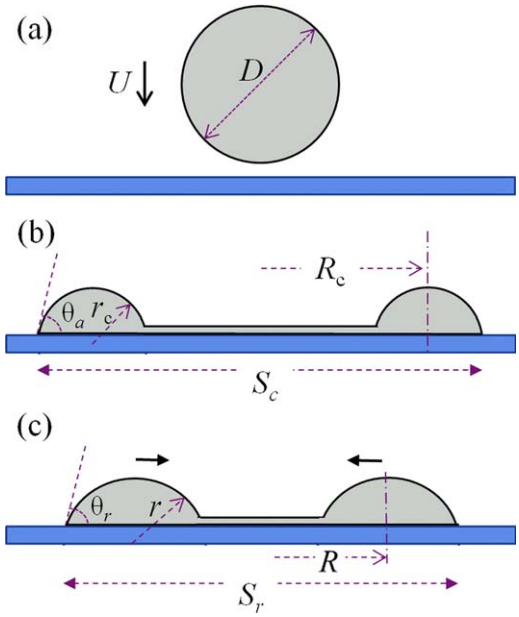

Figure 3. Analytic model of droplet impact (a) droplet falling on a solid surface; (b) maximum spread; and (c) recoiling.

described as a semicircular rim surrounding a thin liquid film, and the shape remains until the disappearance of the liquid film. The semicircular rim has a radius r, and another radius R is from the center of the rim to the center of the ring. As most fluid exists in the rim, we assume the central liquid film has zero volume, but its surface energy must be taken into account. Hence, this geometric model based on the volume conservation is expressed by

$$\frac{1}{2}r^2(2\theta-\sin 2\theta)2\pi R=\frac{\pi D^3}{6} \tag{1}$$

where θ is the apparent contact angle and D is the initial droplet diameter before impact.

Figure 3 also schematically indicates perfect contact between the droplet and the solid surface during both spreading and recoiling processes, which is an important assumption for the theoretical analysis in this work. It has been shown that droplet spread could be significantly affected if an air layer exist between the impacting droplet and the surface.[19] However, by using a high-speed interference imaging technique, a more recent study[20] experimentally demonstrates that no air is trapped beneath the spreading droplet except a small bubble formed at the center of the spreading droplet. For droplet impact without subsequent splashing, if the droplet has been spreading on an air layer during a major portion of the impact process, a relatively big bubble will be formed at the center. However, in this work, droplets spread and recoil smoothly, and no bubbles with visible sizes were observed during and after the impact (see Figure 2). We believe for our study no significant air layer persists beneath the droplet, and it is reasonable to assume perfect liquid–solid contact.

Maximum spread

As shown in Figure 3, the spread diameter at maximum spread is denoted by S_c. To derive a correlation for S_c, we consider the initial and maximum states. The initial state is a free droplet with diameter D approaching the surface with

velocity U (see Figure 3a), and the maximum state is the droplet reaches a maximum spread (see Figure 3b). Clanet et al.[3] found that internal kinetic energy still exists when the drop reaches its maximal extension. However, good prediction was obtained by assuming zero internal kinetic energy.[21] For maximum spread, we neglect remaining kinetic energy but consider potential energy due to nonuniform fluid pressure and surface energy at the instant of maximum state. The viscous dissipation that occurs from the initial state to the maximum state also needs to be considered. Potential energy due to gravity is neglected in this work, as its effect is usually insignificant for momentum-driven droplet impact. Hence, for energy to be conserved at the two states, the following relation needs to be satisfied

$$E_s^0+E_k^0=E_p^c+E_s^c+E_v^c \tag{2}$$

where states 0 and c represent the initial and maximum states. E_s^0 is the surface energy of the droplet prior to impact, and is given by

$$E_s^0=\sigma\pi D^2 \tag{3}$$

Here, σ is liquid–vapor surface tension. The initial kinetic energy of the droplet, denoted by E_k^0, is expressed by

$$E_k^0=\frac{1}{2}\rho\frac{\pi D^3}{6}U^2 \tag{4}$$

where ρ is droplet density. On the right-hand side of Eq. 2, E_p^c is the potential energy at maximum spread, E_s^c is the surface energy, and E_v^c is the viscous dissipation during spreading.

At maximum spread, pressure inside the rim is higher than the rest of the droplet by approximately $\sigma(1/r_c+1/R_c)$. This nonuniform pressure distribution has potential energy expressed as

$$E_p^c\sim\sigma\left(\frac{1}{r_c}+\frac{1}{R_c}\right)\frac{\pi D^3}{6} \tag{5}$$

At maximum spread, surface energy of the droplet is

$$E_s^c=\left[2\theta r_c 2\pi R_c+\pi(R_c-r_c\sin\theta_a)^2\right]\sigma+\pi(R_c+r_c\sin\theta_a)^2(\sigma_{sl}-\sigma_{sv}) \tag{6}$$

The first part on the right-hand side is the surface energy of the total liquid–vapor interface. The second part is the change of surface energy due to the newly formed liquid–solid interface. For maximum spread, the relation between the three interfacial surface tensions satisfy

$$\sigma\cos\theta_a=\sigma_{sv}-\sigma_{sl} \tag{7}$$

which can be used to replace the solid–liquid and solid–vapor surface tensions in Eq. 6. It should be noted that Eq. 7 is a modified Young's equation, where the apparent dynamic angle has replaced the equilibrium contact angle. It is believed that using the dynamic contact angle is more suitable for analyzing the dynamics of droplet impact than using the equilibrium contact angle. This can also be found in previous work.[9]

For viscous dissipation during spreading, we consider the following relation

$$E_v^c\sim\mu\int_{t_c}\left(\frac{U}{\delta_s}\right)^2\Omega\,dt \tag{8}$$

Here $t_c=8D/3U$ is the time taken to reach maximum spread, and the velocity boundary thickness is $\delta_s=2\sqrt{D\mu/\rho U}$.[9] The volume Ω is where velocity gradient exists, and can be approximated as $\Omega\sim\pi(R_c+r_c\sin\theta_a)^2\delta_s$. Hence, Eq. 8 can be further simplified as

$$E_v^c\sim\frac{4\pi}{3}\rho U^2\frac{D}{\sqrt{Re}}(R_c+r_c\sin\theta_a)^2 \tag{9}$$

Inserting Eqs. 3–6 and 9 into Eq. 2, and dividing both sides of Eq. 2 by $\pi D^2\sigma$, the following nondimensional equation is obtained

$$1+\frac{We}{12}=\frac{1}{6}\left[\frac{1}{\hat{r}_c}+\frac{1}{\hat{R}_c}\right]+4\theta_a\hat{r}_c\hat{R}_c+\left(\hat{R}_c-\hat{r}_c\sin\theta_a\right)^2+\left(\hat{R}_c+\hat{r}_c\sin\theta_a\right)^2\left(\frac{4}{3}\frac{We}{\sqrt{Re}}-\cos\theta_a\right) \tag{10}$$

where $We=\rho U^2D/\sigma$ is Weber number, $\hat{r_c}=r_c/D$, and $\hat{R}_c=R_c/D$.

The dimensionless form of Eq. 1 becomes

$$6\hat{r}_c^2\hat{R}_c(2\theta_a-\sin 2\theta_a)=1 \tag{11}$$

Then, Eqs. 10 and 11 are coupled to solve for $\hat{r_c}$ and $\hat{R}_c$. And nondimensional spread diameter, which has been normalized by the droplet diameter D, is given by

$$\hat{S}_c=2\left(\hat{R}_c+\hat{r}_c\sin\theta_a\right) \tag{12}$$

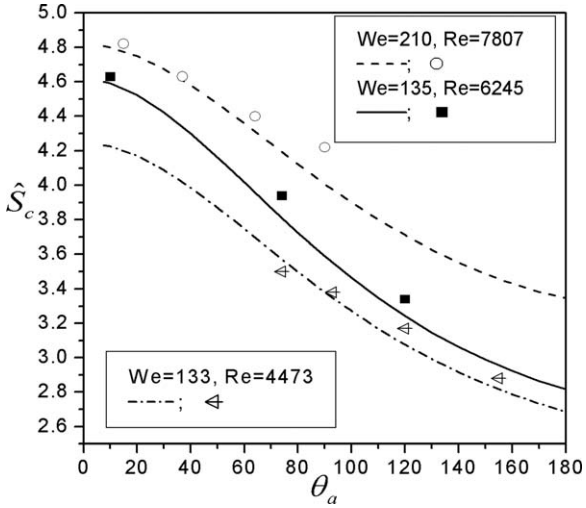

Figure 4. Theoretical prediction (shown as lines) of maximum spread diameter, which has been normalized by the droplet diameter *D*, in comparison with experimental results (shown as scattered symbols).

Figure 4 shows theoretical prediction of maximum spread diameters as compared with experimental results for varied advancing contact angles and droplet impact inertias (Weber and Reynolds numbers). Each experimental data point represents the maximum spread diameter measured from on single test, which has been normalized by the diameter of the droplet. It can be seen that the theoretical model generally agrees well with the experiments. Droplets with large values of Weber and Reynolds numbers tend to spread to larger extents. The influence of Reynolds number on droplet spread is obvious from the comparison between $Re=4473$ and $Re=6245$, for which their values of Weber number are almost equal. The effect of surface wettability can also be seen from Figure 4, where the advancing contact angle

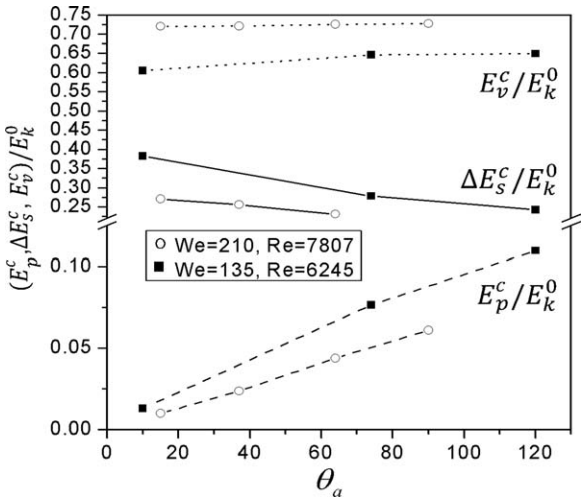

Figure 5. Energy transformation from initial state to maximum state (dotted lines: viscous dissipation; solid lines: excessive surface energy; and dashed lines: flow potential energy).

***Y* axis break is used so that the two dashed lines of potential energy can be clearly shown.**

ranges from 10° to 150°. The maximum spread gradually increases with decreasing the advancing contact angle, which is consistent with the experimental results of Mao et al.[8] and Ford and Furmidge.[22] Under the same impact condition, a larger advancing contact angle leads to a smaller spread diameter.

The maximum spread is a result of energy transformation governed by Eq. 2. If, we define excessive surface energy as $\Delta E_s^c = E_s^c - E_s^0$, Eq. 2 indicates that at the end of the spreading process the initial kinetic energy of the droplet splits into flow potential energy, excessive surface energy, and viscous dissipation. The viscous dissipation is irreversible, whereas excessive surface energy and flow potential energy can be considered reversible, as they will transform to kinetic energy accompanied by viscous dissipation during recoiling.

Figure 5 shows the portions of the three types of energies at maximum spread for two impact inertias on varied surfaces. This is easily obtained by dividing the corresponding terms on the right-hand side of Eq. 10 by the left-hand side of the same equation. First, for droplets with higher impact inertia ($We = 210$), around 70% of their initial energy E^0 was dissipated due to viscosity, around 10% higher than the droplets with lower impact inertia ($We = 135$). As a result, there are less portions of reversible energy for the droplets with higher impact inertia. Second, the portions for viscous dissipation (E_v^c/E_k^0) generally stay constant for varied angles, θ_a. However, the excessive surface energy ($\Delta E_s^c/E_k^0$) decreases with θ_a, whereas the flow potential energy (E_p^c/E_k^0) shows an opposite trend. Around 10% increase of $E_p^c/E^0$is visible for the droplets with $We = 135$ over the range of θ_a from 15 to 120°. Clearly, the flow potential energy becomes significant for surfaces with large advancing contact angles. We tend to believe that the increase of flow potential energy is the major reason for strong rebound of droplets previously observed for hydrophobic and superhydrophobic surfaces. Our results of droplet recoiling in the next section also show faster recoiling on the hydrophobic surfaces.

To further validate our analytical model, Figure 6 shows the comparison of theoretical prediction with experimental results from this work as well as previous work by Ford and Furmidge,[22] who tested the impact of water droplets on different smooth surfaces. Without any adjustable parameter in the model, prediction of maximum spread diameter is in good agreement with the experimental results.

Recoiling

Figure 7 shows a water droplet recoiling on a solid surface after reaching its maximum spread at a nondimensional time $\hat{t} = tU/D = 0$. During the recoiling process, the contact line recedes toward the droplet center, and the spread diameter gradually decreases, and the rim radius increases. The fluid kinetic energy increases due to the decrease of surface energy and flow potential energy. If its kinetic energy is large enough, the droplet can bounce off the solid surface. Capillary waves are visible on the central film. However, for the simplicity of the analysis, we assume the central film has zero volume and smooth surface. Hence, flow energy exists only in the rim of the recoiling droplet, while the central film has only surface energy. The analytical model for recoiling has been depicted by Figure 3c. In this work, our analysis focuses on the recoiling process prior to the disappearance of the central film.

When the droplet starts recoiling, the contact angle changes from advancing contact angle to receding contact angle θ_r. Hence, the radius of curvature of the rim at the initial point of recoiling r_i can be obtained from

$$r_i^2(2\theta_r - \sin 2\theta_r) = r_c^2(2\theta_a - \sin 2\theta_a) \tag{13}$$

And the initial value of R for recoiling is R_c at maximum spread. Based on experimental observation, we assume constant dynamic contact angle during recoiling, which is the receding contact angle, θ_r. Hence, Eq. 1 can be rewritten as

$$\frac{1}{2}r^2(2\theta_r - \sin 2\theta_r)2\pi R = \frac{\pi D^3}{6} \tag{14}$$

For a recoiling droplet, there are flow potential energy E_p^r, kinetic energy E_k^r, surface energy E_s^r, and viscous dissipation E_v^r. Hence, the conservation of energy requires

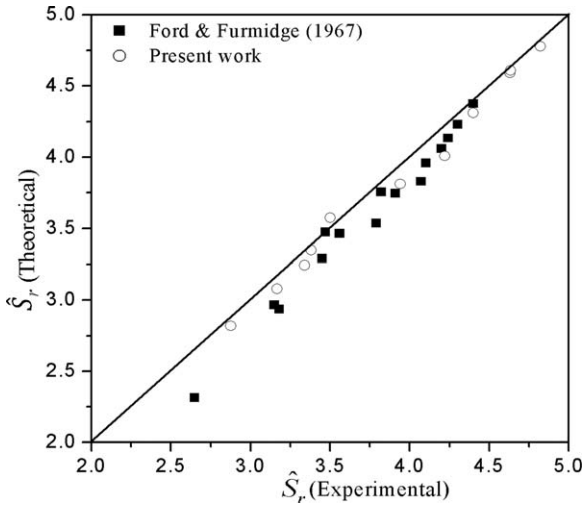

Figure 6. Theoretical prediction of maximum spread diameter vs. present and previous experimental results.

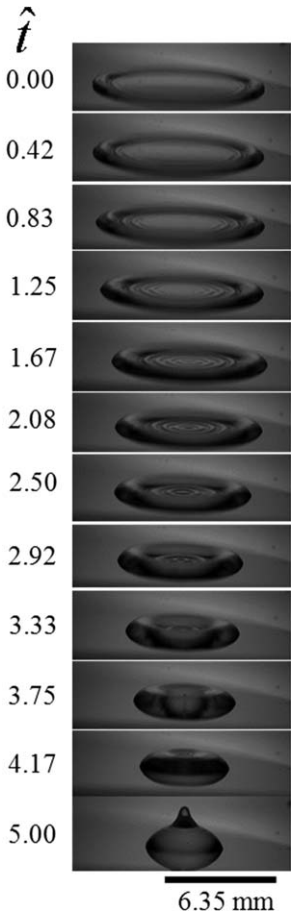

Figure 7. A droplet (U=1.6 m/s; D=3.84 mm) recoils after reaching maximum spread on a smooth surface (θ_a=120°; θ_r=100°) at a nondimensional time $\hat{t}=tU/D$=0.

$$\frac{d}{dt}\left[E_p^r+E_k^r+E_s^r+E_v^r\right]=0 \tag{15}$$

Similar to Eq. 5, flow potential energy is

$$E_p^r=\sigma\left(\frac{1}{r}+\frac{1}{R}\right)\frac{\pi D^3}{6} \tag{16}$$

Approximating that the rim is moving inward with a velocity $-dR/dt$, kinetic energy is

$$E_k^r=\frac{1}{2}\rho\frac{\pi D^3}{6}\left(\frac{dR}{dt}\right)^2 \tag{17}$$

And similar to Eq. 6, surface energy during recoiling is

$$E_s^r=\left[2\theta r 2\pi R+\pi(R-r\sin\theta)^2\right]\sigma+\pi(R+r\sin\theta)^2(\sigma_{sl}-\sigma_{sv}) \tag{18}$$

The interfacial surface tensions during recoiling are assumed to meet

$$\sigma\cos\theta_r=\sigma_{sv}-\sigma_{sl} \tag{19}$$

Similar to Eq. 7, the above relation is another modified Young's equation based on the receding contact angle, and represents a dynamic balance between the three interfacial surface tensions during recoiling.

Table 1. Experimental Tests of Droplets Recoiling and Values of Boundary Layer Coefficient

Test #	Re	We	θ_a	θ_r	λ
#1	4473	133	155	145	0.05
#2	4473	133	120	100	0.23
#3	6245	135	120	100	0.20
#4	4473	133	93	69	0.25
#5	6245	135	74	40	0.21

Now we consider the viscous dissipation during recoiling, which mainly occurs inside the rim. Similar to Eq. 8, we propose

$$E_v^r\sim\mu\int_{t_r}\left(\frac{dR/dt}{\delta_r}\right)^2(\delta_r 2r\sin\theta_r 2\pi R)dt \tag{20}$$

Here δ_r is the boundary layer thickness inside the recoiling rim. And $\delta_r 2r\sin\theta_r 2\pi R$ is the approximate volume where velocity gradient exists. To determine δ_r, we take a look at the boundary layer for spreading $\delta_s=2\sqrt{D\mu/\rho U}$. If the length scale D is replaced by the rim size $r(1-\cos\theta_r)$, and the impact velocity U is replaced by the receding velocity $-dR/dt$, δ_r can be approximately expressed by

$$\delta_r\sim\lambda\sqrt{\frac{\mu}{\rho}\frac{r(1-\cos\theta_r)}{-dR/dt}} \tag{21}$$

Here, a boundary layer coefficient λ is introduced, the value of which will be determined by fitting with experimental data. Inserting Eq. 21 into Eq. 20 gives

$$E_v^r\sim\frac{1}{\lambda}\sqrt{\rho\mu}\int_{t_r}\left(-\frac{dR}{dt}\right)^{5/2}4\pi r^{0.5}R\frac{\sin\theta_r}{\sqrt{1-\cos\theta_r}}dt \tag{22}$$

And then

$$\frac{dE_v^r}{dt}\sim\frac{4\pi}{\lambda}\sqrt{\rho\mu}r^{0.5}R\frac{\sin\theta_r}{\sqrt{1-\cos\theta_r}}\left(-\frac{dR}{dt}\right)^{5/2} \tag{23}$$

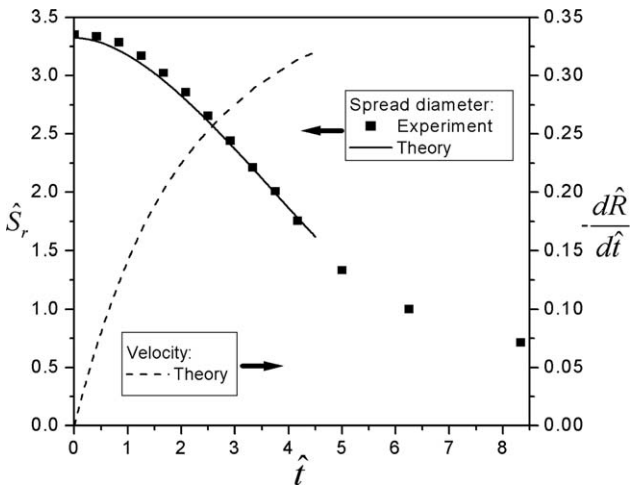

Figure 8. Spread diameter (left *Y* axis) and receding velocity (right *Y* axis) of a water droplet recoiling on a smooth surface (the same test as shown in Figure 7 and Test #3 in Table 1).

The theoretically predicted recoiling stops when the central film vanishes.

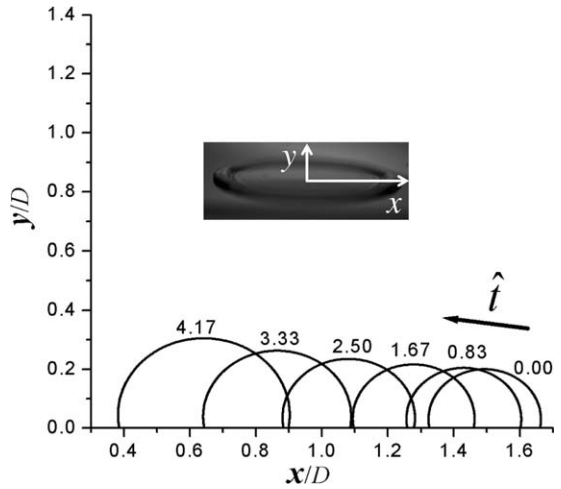

Figure 9. Theoretical prediction of the evolution of the rim during recoiling (Test #3).

Now we substitute Eqs. 16–18 and 23 into Eq. 15, and divide through by $\pi D^2\sigma$. We get

$$\frac{d}{d\hat{t}}\left[\frac{1}{6}\left(\frac{1}{\hat{r}}+\frac{1}{\hat{R}}\right)+\frac{We}{12}\left(\frac{d\hat{R}}{d\hat{t}}\right)^2+4\theta_r\hat{r}\hat{R}\right.$$
$$\left.+\left(\hat{R}-\hat{r}\sin\theta_r\right)^2-\cos\theta_r\left(\hat{R}+\hat{r}\sin\theta_r\right)^2\right] \quad (24)$$
$$+\frac{4}{\lambda}\frac{We}{\sqrt{Re}}\frac{\sin\theta_r}{\sqrt{1-\cos\theta_r}}\hat{r}^{0.5}\hat{R}\left(-\frac{d\hat{R}}{d\hat{t}}\right)^{5/2}=0.$$

Accordingly, Eq. 14 becomes

$$6\hat{r}^2\hat{R}(2\theta_r-\sin 2\theta_r)=1 \quad (25)$$

Apparently Eq. 24 requires three initial conditions, which are

$$\hat{r}_i=\hat{r}_c\left(\frac{2\theta_a-\sin 2\theta_a}{2\theta_r-\sin 2\theta_r}\right)^{0.5}$$
$$\hat{R}_i=\hat{R}_c$$
$$\left(d\hat{R}/d\hat{t}\right)_i=0$$

The first initial condition is from Eq. 13. For the first two initial conditions, r_c and R_c are from theoretical predictions given by Eqs. 10 and 11.

Solving Eqs. 24 and 25 together, the spread diameter during recoiling is

$$\hat{S}_r=2\left(\hat{R}+\hat{r}\sin\theta_r\right) \quad (26)$$

It should be noted the major constraint of the model is $\hat{R}-\hat{r}\sin\theta_r\geq 0$, as the recoiling process considered here is from maximum spread to the point when the central film vanishes. Therefore, the theoretically predicted recoiling needs to stop when the central film vanishes. Additionally, the value of λ needs to be determined by fitting with experimental results for the largest R-squared value.

Five tests of droplet recoiling are reported in the present work as shown in Table 1. The five tests involve varied impact inertias and different substrate surfaces. The values of λ for each case are also determined when the prediction of the spreading diameter during recoiling is in good agreement with the experimental measurement. For #1 test, a textured superhydrophobic surface was used, and a very small value was determined for the boundary layer coefficient. For all other smooth surfaces, it is difficult to correlate the value to either contact angles or droplet impact inertia. But generally, the values are approximately around 0.2.

Figure 8 shows the theoretical prediction and experimental data of Test #3, for which the images of recoiling have been presented in Figure 7. The theoretical curves stop at $\hat{t}\sim 4.5$, when the central film vanishes. As recoiling starts, the spread diameter gradually decreases toward the droplet center while the receding velocity in the radial direction rapidly increases. This indicates accelerated receding of contact line prior to the disappearance of central film. The increase of kinetic energy is due the energy transformation from surface energy and flow potential energy. After the central film disappears, the recoiling decelerates, which is clear from the

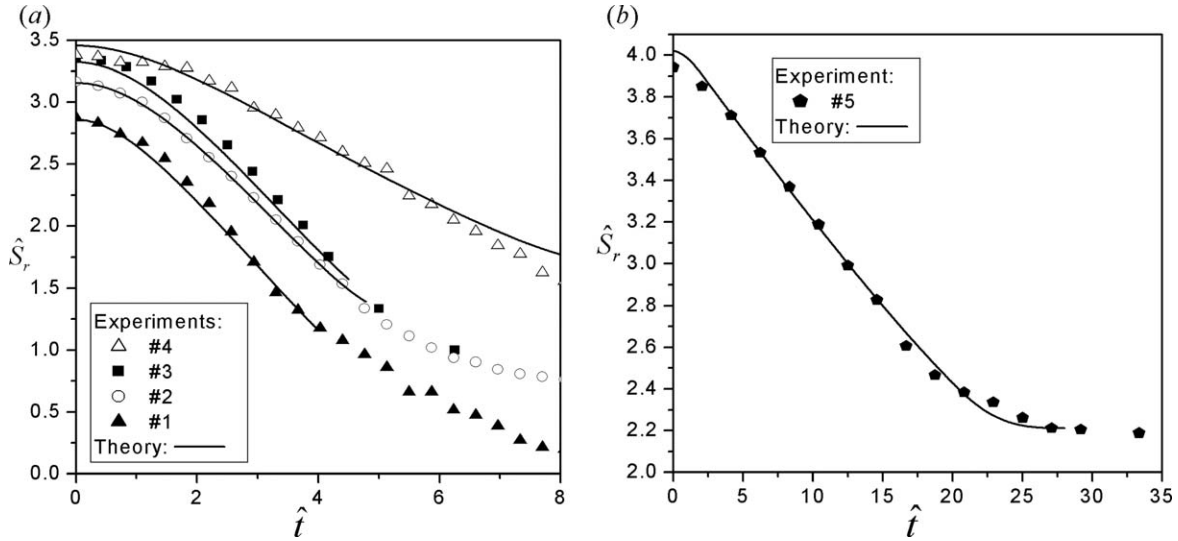

Figure 10. Theoretical prediction of spread diameter during recoiling in comparison with experimental results (details of test conditions are given in Table 1).

experimental data. Figure 9 shows the rim at varied nondimensional time points, where the location of the rim and rim radius are predicted by the theoretical equations. When the droplet starts recoiling, the droplet has a minimum rim radius and a maximum spread diameter. During recoiling, the rim continuously grows as it moves closer to the center of the ring. The evolution of the rim shown in Figure 9 agrees with the experimental observation shown in Figure 7.

Figure 10 shows all the recoiling tests listed in Table 1 in comparison with theoretical prediction. Surface wettability is found to be a significant factor on droplet recoiling. For Tests #1, 2, 4, droplets with the same impact inertia impact different substrate surfaces. In Test #4, the droplet impacting a hydrophilic surface ($\theta_r=69^\circ$) reaches a large maximum spread and then recoils very slowly. The superhydrophobic surface ($\theta_r=145^\circ$) was used for Test #1. The droplet produces a small maximum spread and shows a fast recoiling process. The significant influence of surface wettability can also be shown by comparing Tests #3 and 5, which have the same values of *Re* and *We*. In Test #5, the droplet shows a long recoiling process on a hydrophilic surface ($\theta_r=40^\circ$). It takes six times longer for the central film to vanish as compared to Test #3, for which a hydrophobic surface $\theta_r=100^\circ$ was used. The influence of droplet impact inertia can be discussed by comparing Tests #2 and 3, for which the same surface was tested with different droplet inertias. Despite the different maximum spread diameters at the beginning of the recoiling process, the two droplets exhibit similar recoiling trends.

Conclusions

An experimental and theoretical study on the impact of water droplets on solid surfaces is presented. Droplets with varied sizes and velocities are tested on different surfaces. Except one surface textured for increasing hydrophobicity, all other surfaces are smooth and coated with different SAMs to achieve varied advancing and receding contact angles. The focus is put on the spread diameter at maximum spread and subsequent recoiling. Theoretical predictions are found to agree well with experimental data.

Our experimental observation shows that during impaction the droplet maintains a ring-like shape, which contains a semicircular rim with a thin central film. This shape remains at maximum spread and during subsequent recoiling until the central film vanishes. Both theoretical equations for predicting the maximum spread diameter and receding spread diameter during recoiling are developed based on this shape. For both equations, a flow potential energy term is introduced to take into account the nonuniform distribution of pressure inside the deformed droplet. Additionally, for spreading and recoiling, the Young's equation is modified by replacing the equilibrium contact angle with advancing and receding contact angles, respectively.

When deriving the viscous dissipation term for recoiling, a viscous layer coefficient is introduced, and its value needs to be determined by fitting with experimental data. It was found that the coefficient is around 0.2 for all the tests using smooth surfaces, whereas a very low value of 0.05 was obtained for the test using the superhydrophobic surface.

Surface wettability was found to have significant influence on droplet impact. The maximum spread diameter decreases with increasing advancing contact angle. Droplets recoil faster on surfaces with large receding contact angles, while slow recoiling occurs on surfaces with small receding contact angles. The surface effect may be explained by analyzing energy transformation from initial state to maximum spread state. At maximum spread, surface energy was found to decrease with increasing advancing contract angle, whereas flow potential energy shows an opposite trend.

The theoretical models presented here have their limitations. The first limitation is that the central volume is assumed to be zero volume. This assumption could cause reduced prediction accuracy for droplets impacting with high inertia or on surfaces with high wettability, for which much fluid would exist in the central film due to large spread. The second is that the recoiling model covers only the early portion of the recoiling process, which is before the disappearance of the central film. The third is the viscous layer coefficient introduced in the recoiling model. Although it was found it is around 0.2 for smooth surfaces, further work is still needed to determine its value. All the limitations will be the objectives for our future studies.

Acknowledgments

The authors would like to thank the support by Natural Sciences and Engineering Research Council of Canada (NSERC).

Literature Cited

1. Rioboo R, Tropea C, Marengo M. Outcomes from a drop impact on solid surfaces. *Atomization Spray*. 2001;11:155–166.
2. Li R, Ashgriz N, Chandra S. Maximum spread of droplet on solid surface: low Reynolds and Weber numbers. *J Fluids Eng*. 2010;132:061302.
3. Clanet C, Beguin C, Richard D, Quere D. Maximal deformation of an impacting drop. *J Fluid Mech*. 2004;517:199–208.
4. van Dam DB, Clerc CL. Experimental study of the impact of an ink-jet printed droplet on a solid substrate. *Phys Fluids*. 2004;16:3403–3414.
5. Park H, Carr WW, Zhu JY, Morris J F. Single drop impaction on a solid surface. *AIChE J*. 2003;49:2461–2471.
6. Engel OG. Waterdrop collision with solid surface. *J Res Natl Bur Stand*. 1955;54:281–298.
7. Chandra S, Avedisian CT. On the collision of a droplet with a solid surface. *Proc R Soc London*. 1991;432:13–41.
8. Mao TD, Kuhn CS, Tran HN. Spread and rebound of liquid droplets upon impact on flat surfaces. *AIChE J*. 1997;43:2169–2179.
9. Pasandideh-Fard M, Qiao YM, Chandra S, Mostaghimi J. Capillary effects during droplet impact on a solid surface. *Phys Fluids*. 1996;8:650–660.
10. Kendall GE, Rohsenow WM. Heat transfer to impacting drops and post critical heat flux dispersed flow. Technical Report No. 85694-100. Cambridge, MA: Dept. Mechanical Eng., MIT, 1978.
11. Bechtel SE, Bogy DB, Talke FE. Impact of liquid drop against a flat surface. *IBM J Res Dev*. 1981;25:963–971.
12. Kim HY, Chun JH. The recoiling of liquid droplets upon collision with solid surfaces. *Phys Fluids*. 2000;13:643–659.
13. Roisman IV, Rioboo R, Tropea C. Normal impact of a liquid drop on a dry surface: model for spreading and receding. *Proc R Soc London Ser A*. 2002;458:1411–1430.
14. Suzuki S, Nakajima A, Yoshida N, Sakai M, Hashimoto A, Kameshima Y, Okada K. Freezing of water droplets on silicon surfaces coated with various silanes. *Chem Phys Lett*. 2007;445:37–41.
15. Huang YC, Hammitt FG, Yang WJ. Hydrodynamic phenomena during high-speed collision between liquid droplet and rigid plane. *J Fluids Eng*. 1973;95:276–292.
16. Fukai J, Shiiba Y, Yamamoto T, Miyatake O. Wetting effects on the spreading of a liquid droplet colliding with a flat surface: experiment and modeling. *Phys Fluids*. 1995;7:236–247.

17. Richard D, Quere D. Bouncing water drops. *Europhys Lett*. 2000;50: 769–775.
18. Fukai J, Tanaka M, Miyatake O. Maximum spread of liquid droplets colliding with flat surfaces. *J Chem Eng Jpn*. 1998;31:456–461.
19. Mandre S, Mani M, Brenner MP. Precursors to splashing of liquid droplets on a solid surface. *Phys Rev Lett*. 2009;102:134502.
20. Driscoll MM, Nagel SR. Ultrafast interference imaging of air in splashing dynamics. *Phys Rev Lett*. 2011;107:154502.
21. Bennet T, Poulikakos D. Splat quench solidification: estimating the maximum spread of a droplet impacting a solid surface. *J Mater Sci*. 1993;28:963–970.
22. Ford RE, Furmidge CGL. Impact and spreading of spray drops on foliar surfaces. *Soc Chem Ind Monogr*. 1967;25:417–432.

Manuscript received Oct. 22, 2013, and revision received Feb. 15, 2014.